https://doi.org/10.5194/tc-2020-342
Preprint. Discussion started: 5 January 2021

The Cryosphere Discussions

Reconstruction of annual accumulation rate on firn synchronizing H_2O_2 concentration data with an estimated temperature record

Jandyr M. Travassos[1], Saulo S. Martins[2], Mariusz Potocki[4,5], and Jefferson C. Simões[3,4]

[1]Graduate Program in Geophysics, Universidade Federal do Pará (UFPA), Rua Augusto Corrêa n. 01, Belém, Pará, Brazil
[2]Graduate Program in Geology, Universidade Federal Rural do Rio de Janeiro (UFRRJ). BR-465 Km 7, Seropédica, Brazil
[3]Centro Polar e Climatico, Universidade Federal do Rio Grande do Sul (UFRGS), Porto Alegre, Brazil
[4]Climate Change Institute, University of Maine, Orono, USA
[5]School of Earth and Climate Sciences, University of Maine, Orono, ME 04469, USA

Correspondence: Saulo S. Martins (ssmsaulo@gmail.com)

Abstract. This work deals with two distinct datasets, a well preserved hydrogen peroxide, H_2O_2, concentration data from firn cores at a high deposition location and a temperature time series, estimated from the daily records from four Antarctic stations around the Antarctic Peninsula. With them we have produced a time scale, an ice-core chronology, for the 133m deep borehole DP-07-1 from Plateau Detroit, Antarctic Peninsula. We constructed the chronology through a non-linear pairing transformation of the two series, based entirely on mathematical optimization, compensating the peroxide frequency scaling, reflecting the gradual thinning of the annual firn layers with depth. We resorted to a dynamic time warping algorithm to find an optimal alignment between the two data series, allowing for the thinning of the annual firn layers with depth and the estimation of their original thicknesses at time of deposition. The core chronology spanning from Jan-1980 to Dec-2010 for the borehole reach, a time frame of a mere 30 years period, revealing a fairly stable 11 year average for the accumulation rate of $2.5\,\mathrm{m\,w.e./y}$.

1 Introduction

Ice cores provide a continuous record of climatic and environmental data series based on some physical and chemical properties of ice, reflecting past atmospheric composition and climatic variability, *e.g.* Masson-Delmotte et al. (2006). A key issue in the paleoclimatic reconstruction is dating the stratigraphic sequence through different techniques which include 1-D to 3-D flow models (Nye, 1952; Dansgaard and Johnsen, 1969; Gillet-Chaulet et al., 2012; Passalacqua et al., 2016), counting of cycles of seasonally varying quantities, reference horizons, most commonly layers of high concentrations of sulphuric acid related to volcanic events (Vinther et al., 2006), and layer identification through peaks of radiactive isotopes (Vinther et al., 2006; Cuffey and Paterson, 2010). Often those techniques are combined, *e.g.*, incorporating stable water isotope $\delta^{18}O_{atm}$ to an ice flow model (Capron et al., 2010).

The H_2O_2 is produced by photochemical reactions in natural waters exposed to solar irradiation, surficial and atmospheric. It is the most stable of the reactive oxygen species created in the atmosphere through a chemical reaction requiring ultraviolet light. A kinetic model explained 76.7% of the variation in H_2O_2 concentrations is due to solar irradiance and temperature variation only (Sigg and Neftel, 1988). In particular that production in Antarctica has a conspicuous regular seasonality result-

https://doi.org/10.5194/tc-2020-342
Preprint. Discussion started: 5 January 2021


The Cryosphere Discussions

ing from cycles of complete darkness in midwinter to 24h daylight in midsummer. This gives a phenomenological basis for a quasi-sinusoidal variability in H_2O_2 atmospheric concentration with maxima occurring during the sunlit summer (Steig et al., 2005; Frey et al., 2006). The H_2O_2 reportedly may reach a summer-to-winter ratio of 5 in high accumulation rate ice cores from atmospheric concentration ratios of ~ 50 (Sigg and Neftel, 1988; Hutterli et al., 2003; Frey et al., 2006). The H_2O_2 is a particularly robust marker for ice cores at high accumulation sites in Antarctica (Sigg and Neftel, 1988; Frey et al., 2006).

The H_2O_2 concentration data comes from ice cores extracted from borehole DP-07-1 drilled in December 2007 at the ice divide of Plateau Detroit (PD), at $64°05'07''S$, $59°38'42''W$, $1930\mathrm{m}$ above sea level. DP-07-1 reveals well-resolved seasonal cycles of H_2O_2 concentration data on a context of a very high deposition rate (Potocki et al., 2016). We take advantage of the observed strong seasonality in the H_2O_2 record to estimate a core time scale spanning the entire firn horizon. That is done through the synchronization of the concentration data to an estimated temperature time series at the borehole location.

The reported strong seasonality on the production of H_2O_2 in Antarctica, allow us to concentrate on the yearly cycles of the surficial atmospheric temperature alone as a proxy for the solar irradiation. A temperature record at the borehole location on PD may be estimated by interpolating the historical temperature recordings from six Antarctic stations, not too far from PD: Bellingshausen, Esperanza, Faraday, Marambio, O'Higgins and Rothera, which have almost continuous meteorological observations from the late 1950's. We have discarded Bellingshausen and O'Higgins, the first for being heavily biased by maritime conditions, the second due to a relatively short record with a sizable gap in it, leaving us with four stations forming the vertices of a polygon having PD within its perimeter. Only Marambio lies on the eastern side, which may imply some unknown bias towards the western temperature regime of the Antarctic Peninsula. Figure 1 shows the locations of the Antarctic stations on an outline of the Northern Antarctica Peninsula.

The synchronization of the concentration data to a temperature series is warranted here due to the local accumulation rate, high enough to bring the entire firn horizon deposition period to within the reach of the four stations operational span. Both data series independently follow the same seasonal variation, the passing of the years, nevertheless in their particular manners; the H_2O_2 concentration displays a frequency scaling with depth, a result from the accumulated vertical strain, whereas the temperature series has an uniform frequency behavior. The frequency scaling reflects the gradual thinning of the annual firn layers, which manifests itself as a frequency chirp in the H_2O_2 concentration series.

We have allowed for the frequency scaling of the peroxide concentration series in relation to the uniform frequency temperature content by resorting to dynamic time warping (DWT). The DWT is a fast and efficient algorithm for finding an optimal alignment between two sequences through a non-linear warping of one onto the other along the time/depth axis (Rabiner et al., 1978; Sakoe and Chiba, 1978). We have worked with standardized versions of the peroxide and temperature series, using the distance between them as a measure for their resemblance (Rabiner et al., 1978; Sakoe and Chiba, 1978). Once this is optimally found, the peroxide series becomes warped onto the temperature series thus allowing for the observed frequency scaling.

Notwithstanding DTW has begun associated with speech recognition (Rabiner et al., 1978; Sakoe and Chiba, 1978; Gilbert et al., 2010) it has proved to be useful in several other applications. They encompass handwriting recognition (Kolhe et al., 2009), image and shape matching (Wang et al., 1997; Latecki et al., 2007), analysis and classification the land cover of remotely

https://doi.org/10.5194/tc-2020-342
Preprint. Discussion started: 5 January 2021

The Cryosphere
Discussions
Open Access
EGU

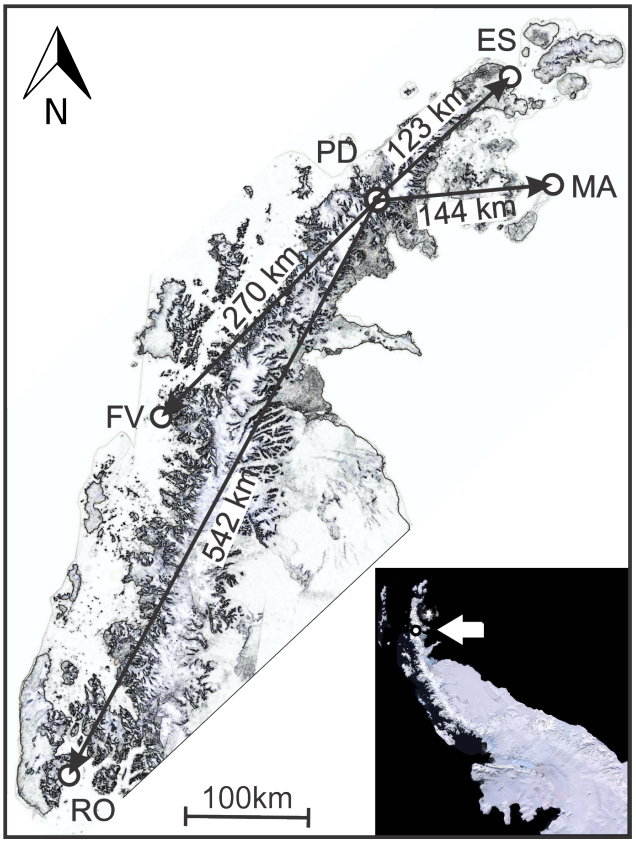

Figure 1. The four Antarctic Stations, Esperanza (ES), Marambio (MA), Faraday-Vernadsky (FV) and Rothera (RO), and of the borehole at PD, on the Northern Antarctica Peninsula. The white arrow in the right lower corner inset shows the location of PD on the Peninsula. Both maps were modified from a pan-sharpened scene (RGBREF_x $-$ 2550000y $+$ 1350000) of the Landsat Image Mosaic of Antarctica (LIMA) by USGS https://lima.usgs.gov/

.

sensed images (Verbesselt et al., 2010; Xue et al., 2014), gene expression and protein structure (Criel and Tsiporkova, 2005; Legrand et al., 2008) and even brain activity (Chaovalitwongse and Pardalos, 2008).

This work shows that DTW is also particularly fit for compensating the peroxide frequency scaling with depth, realigning it to a temperature data time series and, at the same time, quantifying their dissimilarities. We have used the constant spectral content of the temperature data series as a reference in the pairing transformation through mathematical optimization, thus yielding an estimate of a relation of depth to time without human intervention. Moreover the procedure has also confirmed a very high deposition rate for the entire firn horizon at PD.

https://doi.org/10.5194/tc-2020-342
Preprint. Discussion started: 5 January 2021


The Cryosphere Discussions

2 The Data Sets

We deal with two independent data sets, a H_2O_2 concentration from the 133m deep borehole and a temperature time series estimated at PD. We have also collected a record of the stable water isotope deuterium, which was not used due to its poor seasonal variability (Potocki et al., 2016). The borehole yielded intact ice cores down to $z = 109.3 \pm 0.5\mathrm{m}$, from where brittle ice begun. The borehole temperature was fairly stable at $-14.2 \pm 0.1\,^{\circ}\mathrm{C}$ at a depth of 10m, conductivity measurements on ice cores down to 20m had a modal value of 40.4μS/cm. Depths in the borehole are measured with the origin at the surface and the vertical z-axis pointing downwards.

The temperature time series at borehole location was estimated through an interpolation procedure on a data set of continuous temperature readings since January 1^{st}, 1970, at four Antarctic stations in Antarctic Peninsula. We are going to show below that the entire firn layer was accumulated in a shorter time span than the $> 45\mathrm{y}$ of estimated temperature time series.

2.1 The H_2O_2 Concentration Data

The H_2O_2 concentration data has a high resolution sampling, averaging to 36 samples/year along the $98\mathrm{m}$ of ice cores. It has a robust seasonal signal, well preserved for the entire depth range (Potocki et al., 2016). As for other ice cores at high accumulation sites across West Antarctica, it is possible to establish a time scale for the core through straightforward counting of the annual cycles (Sigg and Neftel, 1988; Frey et al., 2006).

The H_2O_2 concentration record, $C(z)$ has a considerable noise content throughout, which has to be minimized making its seasonal signal conspicuous. We produce a smooth data series $\mathcal{C}(z)$ by robust fitting on $C(z)$ through a loess nonparametric method (Cleveland and Grosse, 1991). The Figure 2 shows both $C(z)$ and $\mathcal{C}(z)$ in micro molar (μM) concentration. It is easy to see the seasonal signal in $\mathcal{C}(z)$ as well as the effect of the accumulated vertical strain with depth on the annual firn layers. The latter manifests itself as a gradual thinning of the annual firn layers.

Notwithstanding some residual noise left on $\mathcal{C}(z)$ straightforward counting of its peaks and troughs suggests the first $100\mathrm{m}$ were probably accumulated in its entirety from the beginning of the 80's. Straightforward division of the total depth span by the number of peaks indicates a very high deposition rate at PD, a topic we are going to address below.

2.2 Estimating a Temperature Time Series at PD

The four stations shown in Figure 1 have distinct sampling frequencies in their respective temperature records: 3, 4, 8 and $1^{\mathrm{readings}}/_{\mathrm{day}}$, respectively. We set the beginning of the estimated temperature record to January 1^{st}, 1970, from this date onward all four stations have continuous temperature readings. The end of the record is set on December 29^{th}, 2010, three years after the core was drilled at PD. These limits yield a time span wide enough to safely encompass the entire deposition period of the firn horizon.

We interpolated temperature time series from the four stations shown in Figure 1 through Delaunay triangulation, weighted by the inverse of the horizontal distance between a given station to the sea-level projection of the borehole. We have considered only the maximum daily temperature reading at each station. The sea-level interpolated time series at PD, $T(t)$, is further

https://doi.org/10.5194/tc-2020-342
Preprint. Discussion started: 5 January 2021

The Cryosphere
Discussions
Open Access
EGU

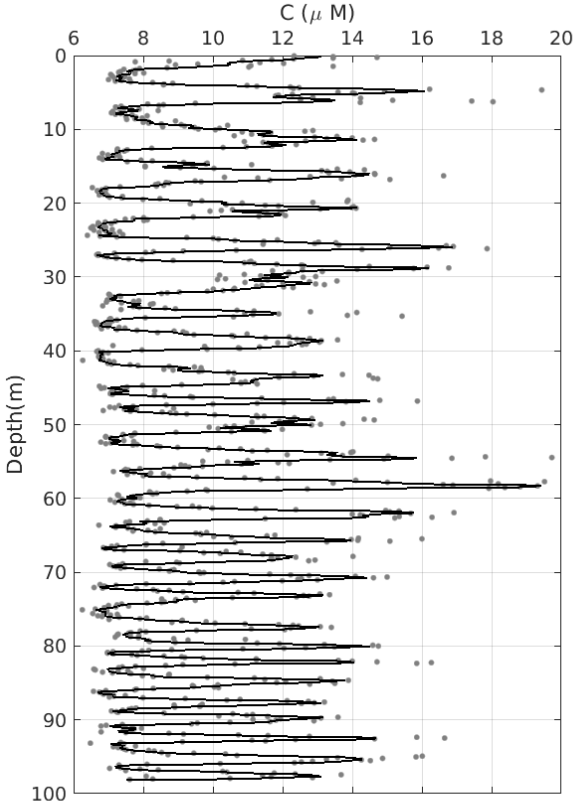

Figure 2. The grey dots are the raw data $C(z)$, the solid line is their smoothed version $\mathcal{C}(z)$, both expressed in μM. For the sake of of visualization we have omitted just two data points with concentration $C(z) > 20\mu$M at depths ≈ 5m.

corrected to the height of PD at $1930\mathrm{m\,asl}$, using a conservative lapse rate for the decreasing of temperature with altitude of $-0.55°\mathrm{C}/100\mathrm{m}$ (Rolland, 2003).

We alleviated aliasing due to the temperature sampling by applying a two-day low-pass filter to $T(t)$, a series with 14973 data points, far more than the 985 data points of $C(z)$. We made the number of data points in $\mathcal{T}(t)$ similar to those in $C(z)$ by decimating the former by $15\times$. Again we avoided aliasing and conspicuously reduced noise in $\mathcal{T}(t)$ by low-pass filtering the decimated data series, using an eight order Chebyshev filter. We compensated the amplitude losses incurred throughout the conditioning process by a constant multiplicative gain, bringing the amplitudes of the filtered temperature time series somewhat back to the original levels of the unfiltered $T(t)$. The multiplicative factor is estimated in successive time windows as the quotient of the envelope of the original $T(t)$ by envelope of the not gained version of $\mathcal{T}(t)$. From now on $\mathcal{T}(t)$ will refer to the gained temperature time series.

https://doi.org/10.5194/tc-2020-342
Preprint. Discussion started: 5 January 2021

The Cryosphere
Discussions
Open Access
EGU

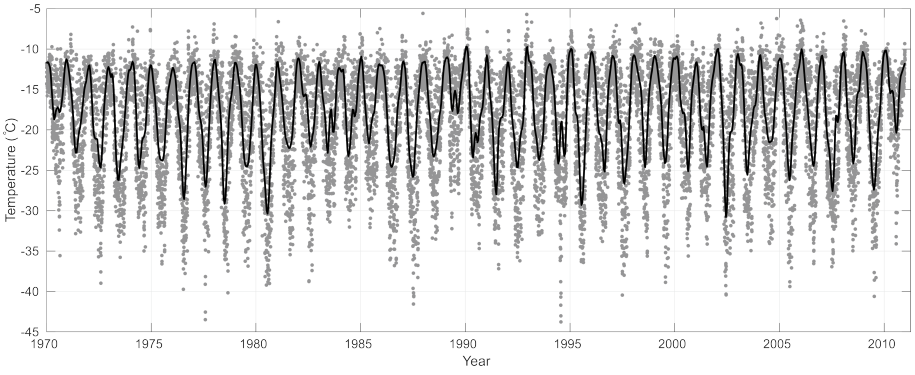

Figure 3. The grey dots are the interpolated and decimated temperature time series $T(t)$. The solid curve is its smoothed and gained counterpart $\mathcal{T}(t)$.

Figure 3 shows the decimated $T(t)$ and $\mathcal{T}(t)$, spanning over 41 years. The time series $T(t)$ is quite noisy as one would have expected it to be but the $\mathcal{T}(t)$ proves to be a robust depiction of the annual summer-winter cycles. It has a smaller amplitude than that of $T(t)$, which is hardly an issue here as we are not looking for individual temperature figures but rather a reliable counter on the passing of the years.

3 Results

3.1 Warping H_2O_2 concentration data onto the Temperature Series

Figures 2 and 3 conspicuously show that the $\mathcal{C}(z)$ and $\mathcal{T}(t)$ data series record the passing of the years through their annual cycles of peaks and troughs, summer to winter respectively. Nevertheless the two data series do record the annual cycles in distinct manners, the former against depth and the latter against time, their similar shapes suggesting we could employ a simple mapping procedure from depth to year of deposition to a common variable related to time.

Two issues to consider here: (i) $\mathcal{C}(z)$ and $\mathcal{T}(t)$ have their respective zeniths at a given summer on distinct dates, as they are distinct phenomena, and (ii) the shape of the two data series conspicuously differ from each other in terms of their spectral characteristics as easily seen comparing Figures 2 and 3. The first issue is easily dealt with as peaks will differ from each other within a fraction of a given summertime, a noise source one just needs to be aware of. The second point is more involved as $\mathcal{T}(t)$ is a function of time with a nearly constant frequency content throughout, whereas $\mathcal{C}(z)$ has a frequency scaling with depth, a chirp behavior easily seen in Figure 2. The latter results from the gradual thinning of the firn layers due to the weight of the overburden.

https://doi.org/10.5194/tc-2020-342
Preprint. Discussion started: 5 January 2021

The two data series $\mathcal{C}(z)$ and $\mathcal{T}(t)$ are not directly comparable, being functions of depth and time. We can make them comparable though by using a standardizing mapping procedure,

$$\begin{aligned} \mathcal{C}_i &\longmapsto \widehat{\mathcal{C}}_i = \tfrac{1}{\sigma(\mathcal{C}_i)}\left(\mathcal{C}_i - \overline{\mathcal{C}}\right) \\ \mathcal{T}_i &\longmapsto \widehat{\mathcal{T}}_i = \tfrac{1}{\sigma(\mathcal{T}_i)}\left(\mathcal{T}_i - \overline{\mathcal{T}}\right), \end{aligned} \tag{1}$$

where $\mathcal{C}_i \equiv \mathcal{C}(z)$ and $\mathcal{T}_i \equiv \mathcal{T}(t)$, $i = 1, \ldots, N$. The $\overline{\mathcal{C}}$ and $\overline{\mathcal{T}}$ are averages and $\sigma(\mathcal{C}_i)$ and $\sigma(\mathcal{T}_i)$ are standard deviations. The two standardized series, $\widehat{\mathcal{C}}$ and $\widehat{\mathcal{T}}$, have the same number of data points and are zero-mean with unit standard deviation. The standardization process minimizes eventual $y-$axis discrepancies between the two series, dwindling the possibility of misalignment by the DTW algorithm. The mapping (1) is invertible, allowing to go back to the original values whenever needed.

Warp the series $\widehat{\mathcal{C}}$, call it the sample, onto the reference series, $\widehat{\mathcal{T}}$, allowing for layer thinning with depth in the sample. In applying DTW we construct a warp path $W = (w_1, w_2, \ldots, w_K)$ between sample and reference, where each path element w_k is linked to the two series indexes (i, i'), for the N elements in $\widehat{\mathcal{C}}$ and $\widehat{T}$, respectively. The warp path length W is bounded to $N \leq K \leq 2N - 1$ and subject to the criteria below.

- Boundary conditions: The warp path start and end at the first and the last elements of the two sequences, $w_1 = (1, 1)$ and $w_K = (N, N)$, all elements considered.
- Continuity: The warping procedure preserves the ordering of the two aligned sequences.

  $$w_k(i, i') \rightarrow w_{k+1}\left(\widehat{i}, \widehat{i'}\right) \Rightarrow i \leq \widehat{i} \leq (i+1) \text{ and } i' \leq \widehat{i'} \leq (i'+1),$$

- Monotonicity: The elements of W are monotonically spaced in the independent variable, thus preventing big jumps.

  $$w_k(i, i') \rightarrow w_{k+1}\left(\widehat{i}, \widehat{i'}\right) \Rightarrow \left(i - \widehat{i}\right) \geq 0 \text{ and } \left(i' - \widehat{i'}\right) \geq 0.$$

The process of warping the sample onto the reference series is done through seeking the path W which yields the minimum-distance,

$$D_W = \frac{1}{2N} \min \left\{ \sum_{k=1}^{K} d(w_k, w_{k+1}) \right\}, \tag{2}$$

where $d(w_k, w_{k+1})$ is the distance between two contiguous elements. DW should attain its minimum when the sample is corrected warped onto the reference signal (Sakoe and Chiba, 1978). We do the DTW through with an algorithm using a correlation optimized warping, or COW, which aligns the sample onto the reference by piecewise linear stretching and compression of the warping segments with variable lengths l (Nielsen et al., 1998; Pravdova et al., 2002; Tomasi et al., 2004).

https://doi.org/10.5194/tc-2020-342
Preprint. Discussion started: 5 January 2021


The Cryosphere Discussions
Open Access
EGU

The range of possible segments l is limited by an integer slack parameter, initially set to unity, $\mathfrak{s} = 1$. The reconstructed sample is obtained by retaining only the highest values obtained for the cumulative correlation coefficient,

$$\xi\left(\widehat{\mathcal{T}},\widehat{\mathcal{C}}\right) = \frac{\sum_l \left(\widehat{\mathcal{T}_{i'}} - \overline{\widehat{\mathcal{T}}}\right)\left(\widehat{\mathcal{C}_i} - \overline{\widehat{\mathcal{C}}}\right)}{(M-1)\,\sigma\left(\widehat{\mathcal{T}_{i'}}\right)\sigma\left(\widehat{\mathcal{C}_i}\right)}, \tag{3}$$

where the summation is performed for each segment l with M points, $\overline{\widehat{\mathcal{T}}}$ and $\overline{\widehat{\mathcal{C}}}$ are averages, and $\sigma\left(\widehat{\mathcal{T}_{i'}}\right)$ and $\sigma\left(\widehat{\mathcal{C}_i}\right)$ are standard deviations. The problem is solved by applying the COW algorithm on all N/l segments through dynamic programming (Nielsen et al., 1998; Pravdova et al., 2002; Tomasi et al., 2004). A complete description of the DTW and COW algorithms is well beyond the scope of this work, the reader is kindly referred to the literature cited herein.

Begin the process of warping $\widehat{C}$ onto $\widehat{T}$ with the two series aligned at their respective beginnings: the borehole bottom and January 1st, 1970, respectively. Warp $\widehat{C}$ and retain the value of the total distance D_W. Discard the year 1970 on $\widehat{T}$, which now begins on January 1st, 1971 and repeat the warping procedure with the entire $\widehat{C}$ record; retain the new vaule for the total distance D_W. Continue moving forward the beginning of the $\widehat{T}$ record in one year steps, storing the values of D_w estimated at each iteration. Continue this process of advancing the beginning the $\widehat{\mathcal{T}}$ in one year steps, monitoring the evolution of the estimated values of D_w.

We observed a decreasing trend in the estimates of D_w retained at each round of warping described above, which reached a conspicuous minimum with the begining of the $\widehat{\mathcal{T}}$ series aligned on January 1st, 1980. Further one-year steps on the starting date of the temperature ensued an increasing trend with a faster pace. We stopped the one-year step warping process on the incresing branch of D_w five years after reaching its minimum. Figure 4 shows both the original and warped versions of series $\widehat{C}$, with the borehole bottom, aligned with $\widehat{T}$ on January 1st, 1980. The Figure also shows the behavior of D_w for the entire year span we have considered in our calculations.

Once $\widehat{T}$ is warped onto $\widehat{C}$ one can easily perform an inverse mapping to the original depths and time, $i = 1, \ldots, N \mapsto (t; z)$. With that depths may be mapped onto time, directely yielding a borehole time scale, $z = z\,(t)$. That is is shown in the lower panel of Figure 4 where $\widehat{C}$ is plotted against deposition time in years. The conspicuous minimum on D_w suggests a quantitative error estimate of $\lesssim 1\mathrm{year}$, significantly greater than any eventual difference between the time of occurrence of the peaks in $\widehat{C}$ and $\widehat{T}$ within a given year.

3.2 Estimating a Borehole Time Scale and an Accumulation Rate

A simple model of an ice sheet flow considers that as an year's snowfall moves downward relative to the surface during its burial process by subsequent deposition undergoing viscoplastic deformation, becoming progressively thinner, extending laterally due to ice incompressibility. An increase in density does ensue with depth as snow slowly compacts itself into firn and from that into ice. One way to simplify the process is to express all lengths in water-equivalent units (mweq), thus allowing one to disregard the compaction of snow *before* the complete transformation to ice. Accordingly we present depths as $z_{mweq} = z\,{}^{\rho(z)}/_{\rho_w}$, where $\rho(z)$ and ρ_w are the density measured in the ice cores from PD and of pure water, respectively.

https://doi.org/10.5194/tc-2020-342
Preprint. Discussion started: 5 January 2021

The Cryosphere Discussions
Open Access
EGU

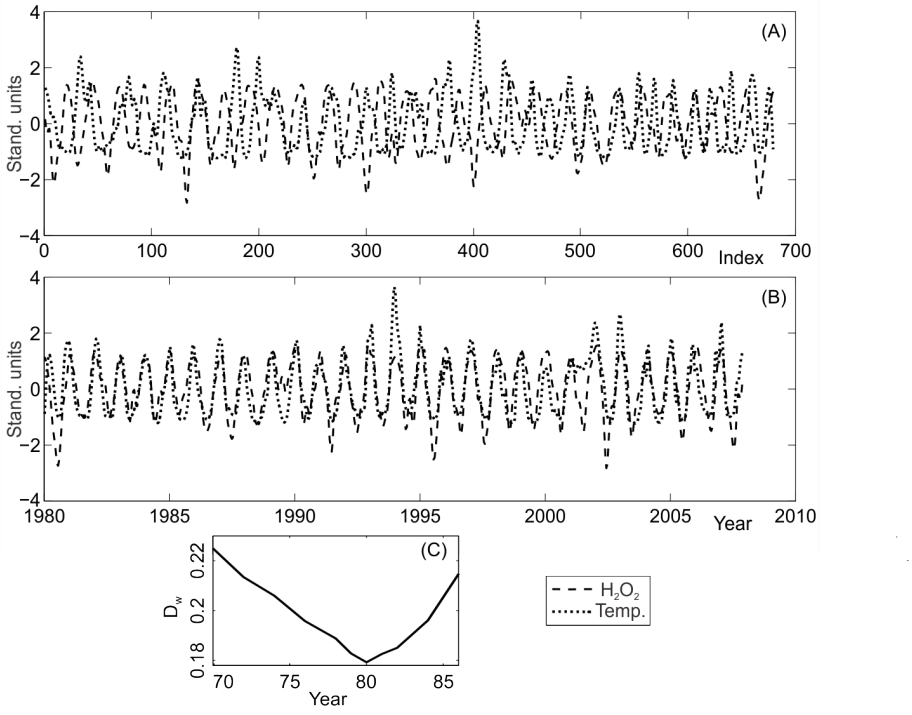

Figure 4. Panel (A) shows the unwrapped $\widehat{C}$ and $\widehat{T}$ series in standardized ordinates, the index $i = 0$ corresponding to the mouth of borehole. Panel (B) shows the two warped series with their abscissas i mapped back to time, expressed in years beginning on January 1st, 1980: $\mathcal{T}, \mathcal{C}(t)$. In both panels $\widehat{C}$ is shown as a dotted curve and $\widehat{T}$ shown as a dash curve, ordinates in arbitrary units. Panel (C) shows the behavior of distance D_w for the year span we have performed the wrappings.

We use the measured $\rho(z)$ from the ice cores to estimate an empirical model of firn densification which assumes the density change with depth is proportional to the deviation relative to the density of pure glacier ice $\rho_{ice} = 0.91 g/cm^3$ (Cuffey and Paterson, 2010). The model may have two (Herron and Langway Jr, 1980) or even three (Ligtenberg et al., 2011) distinct firn densification stages, spanning from the surface to the zone of pore close-off. The adopted model has one densification stage from the surface down to the last available density estimate at $z_{\rho(\max)} = 64.5\mathrm{m}$: $\rho_z = 0.339\, z^{0.1853}$, with $R^2 = 0.97$ (Travassos et al., 2018). The density measurements beyond $z_{\rho(\max)}$ were accidentally lost so we impose the density of glacier ice to the borehole bottom, $\rho(109\mathrm{m}) = \rho_{ice}$, bridging the data gap with a straight line linking the imposed value to the last measured density. This extrapolation will result in some inaccuracies but as at $z_{\rho(\max)} = 64.5\mathrm{m}$ the power law has already reached its slowest increase rate with depth, it may be reasonable to assume they are relatively small. On the other hand that allows for the transformation of length dimensions to mweq for the entire borehole. We will bring this issue back below whenever appropriate.

https://doi.org/10.5194/tc-2020-342
Preprint. Discussion started: 5 January 2021

In the simplest model for an ice sheet flow the total vertical strain of any layer is equal to the total vertical strain of the ice beneath it,

$$\frac{\lambda(z)}{\lambda_0} = \frac{(1-z)}{h}, \tag{4}$$

of a layer of thickness $\lambda(z)$ since it has been deposited at the surface as an annual layer λ_0 thick and h is the total ice thickness. The model considers a steady state viscoplastic deformation with depth at the center of an ice sheet, as the annual layers are buried by subsequent deposition. From now on all length dimensions are in mweq, unless explicitly said otherwise. As ice sheet is in a steady state we assume that accumulation and vertical thinning are constant in time and that a layer thickness does not vary horizontally. If those assumptions hold the distance an ice particle moves downwards during one year must be equal to the thickness of one annual layer $\lambda(z)$.

As the older ice is closer to the bedrock, it is more convenient to express the vertical position of an ice particle in relation to the rock bed interface using a new vertical axis, $Z = h - z$. The new coordinate frame runs in the opposite direction to the one we have been using so far with $z > 0$ pointing downwards. Assuming a steady state the distance an ice particle moves downwards in one year, or for that matter, the particle vertical velocity $\nu(Z)$, is a linear function on Z and therefore the thinning rate $\mathrm{d}\nu/\mathrm{d}Z$ is constant. The velocity at the surface equals the accumulation rate $\nu(h) = -a$ and at the bed $\nu(0) = 0$, the velocity being negative in the new reference frame as it points downwards,

$$\nu(Z) = -a\frac{Z}{h}. \tag{5}$$

The relation between a given depth Z to the age of ice is given by

$$t = \int_h^Z \nu^{-1}\mathrm{d}Z \longrightarrow Z = h\exp\left(-\frac{a}{h}t\right), \tag{6}$$

known as Nye's time scale (Nye, 1952, 1963; Cuffey and Paterson, 2010). Relation (6) provides the simplest model for describing how a layer of thickness λ_0 deposited at the surface thins to $\lambda(Z)$ when it is at a distance Z from the bed. Notwithstanding its simplicity the Nye model still provides good estimates at shallow depths which are close to the ones from more complex models, such as the Dansgaard-Johnsen model (Dansgaard and Johnsen, 1969; Cuffey and Paterson, 2010).

The warping of $\widehat{C}$ onto $\widehat{T}$ estimates the deposition thickness λ_0 from its observed thickness $\lambda(z)$, therefore yielding a time scale $z(t)$ spanning the entire borehole. The $z(t)$ is shown in Figure 5 is a spline linking the center of each corrected, warped, thickness λ_0 against time. The beginning of the extrapolated densities beyond $64.5\mathrm{m}$, shows as a subtle inflection at ~ 1990.

The annual accumulation over the period 1980-2008 as revealed by the warped thicknesses λ_0 show wider oscillations towards later years, but their 11-year moving average, $\bar{a}_{11y} \cong 2.5\,\mathrm{m\,w.e./y}$ appears fairly stable for the period 1980-2008. Figure 5 also shows the 11-year annual accumulation estimated at Gomez in the south-western Antarctic Peninsula (Thomas et al., 2008), showing that a_{ma} is more than twice as large, a very high accumulation rate.

https://doi.org/10.5194/tc-2020-342
Preprint. Discussion started: 5 January 2021

The Cryosphere Discussions

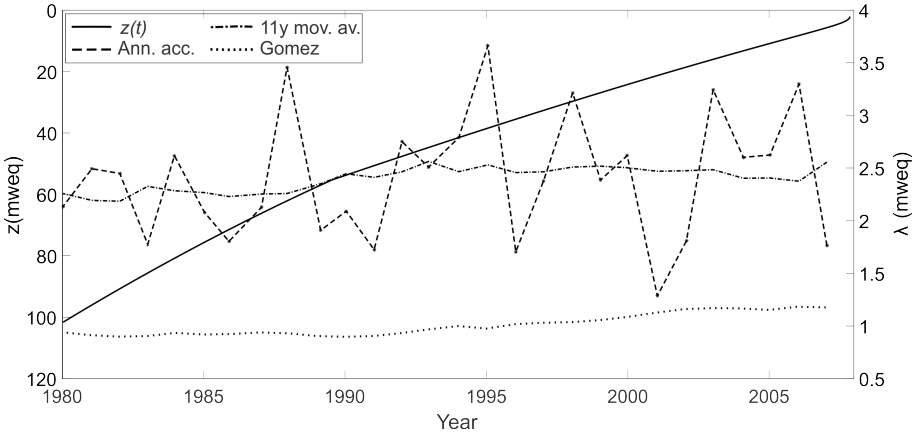

Figure 5. The solid line shows the time scale $z(t)$ (left ordinate) for the firn layer at PD. The dash line shows the annual accumulation rate estimates, the dot-dash line giving their 11-year moving average (right ordinate). The lower dot line shows the 11-year moving average of the annual accumulation rate (right ordinate) at Gomez for comparison (Thomas et al., 2008).

Apply an exponential regression on the warped data to produce estimates for the two constants $(h, {}^{a}/_{h})$ in relation (6). As the available data is confined to the firn layer an estimate for the total thickness h is obviously beyond our reach. Nevertheless as annual accumulation rate is assumed uniform we can obtain an estimate for the the 27 years prior to the coring activity, $a_N = 2.82\,{}^{\text{mweq}}/_{\text{y}}$. The two accumulation rate estimates, a_N and $\bar{a}_{11y}$ are compatible, providing a check on our numerical procedure.

4 Conclusions

We have produced a time scale, an ice-core chronology $z(t)$, for the 133m deep borehole DP-07-1 drilled in Plateau Detroit, Antarctic Peninsula. $z(t)$ is a direct outcome from the process of warping a high resolution H_2O_2 concentration data series onto an estimated local temperature time series. The reliability of the procedure is rooted on the robustness of H_2O_2 as a seasonal marker in a location of high accumulation, which in turn brought the borehole depth span to within the operational life of the Antarctic stations. The non-linear warping of the concentration data onto the estimated temperature record allowed for correcting the thinning of annual layers due to the vertical strain with depth of the firn layers, to obtain an estimate of their thicknesses at the time of snow deposition.

With the warping procedure the annual layers, as revealed through a series of peaks and troughs on the H_2O_2 series, have their thicknesses corrected to their original values at the year of snow deposition. The reconstructed thickness built during one year is equals to the annual accumulation rate. An 11-year moving average of the reconstructed annual layer thicknesses displays a fairly stable behavior throughout the 27 years prior to coring, $\bar{a}_{11y} \cong 2.5\,\text{m w.e.}/\text{y}$. Regressing the same data using the exponential expression of Nye's time scale yields another estimate for the annual accumulation rate, $a_N = 2.82\,\text{m w.e.}/\text{y}$. Those two estimates may be regarded as defining a range for a very high annual accumulation rate. That range points to an

https://doi.org/10.5194/tc-2020-342
Preprint. Discussion started: 5 January 2021


The Cryosphere Discussions

accumulation rate more than 3 times the one reported at Gomez in the south-western Antarctic Peninsula $0.8^{\mathrm{m}_{weq}/\mathrm{y}}$ (Thomas et al., 2008).

By the same token we have taken advantage of the strong seasonality on H_2O_2 data and the high accumulation rate to perform the warping procedure we could have used them to estimate the mean annual accumulation rate by straightforwardly counting the peroxide annual cycles. If one counted the peaks in Figure 2 one would have estimated an accumulation of $a_c = 2.5\,\mathrm{m\,w.e./y}$ as it is reported elsewhere (Potocki et al., 2016). On the other hand one would not have been able to retrieve the time-corrected layer thickness accumulated at the surface at a given year λ_0. All the results related to the accumulation at PD were obtained through a mathematical optimization process, without human intervention.

Author contributions. J. Travassos worked with the synchronization of H_2O_2 and temperature data series and its accrued accumulation rate, and wrote the manuscript. S. Martins estimated the temperature data series and contributed with additional data processing. M. Potocki processed the original H_2O_2 data series from the ice cores. J. Simões worked with all aspects of acquiring the ice cores in the field and contributed with several glaciological aspects of this work. All authors reviewed and agreed on the final manuscript.

Acknowledgements. This work was fully supported by the Brazilian Antarctic Program (PROANTAR), through the CNPq and CAPES. The two main sources come from the INCT da Criosfera (CAPES Proj. 88887.136384/2017-00) and PROANTAR/CNPq (Proj. 442755/2018-0). The present work is part of the ice core program Climate of Antarctica and South America (CASA) in association with the Climate Change Institute, University of Maine. Authors also acknowledge the logistical support of the Chilean Antarctic Institute/INACH and the Chilean Air Force/FACh, the Brazilian Air Force and Navy.

https://doi.org/10.5194/tc-2020-342
Preprint. Discussion started: 5 January 2021

References

Capron, E., Landais, A., Lemieux-Dudon, B., Schilt, A., Masson-Delmotte, V., Buiron, D., Chappellaz, J., Dahl-Jensen, D., Johnsen, S., Leuenberger, M., et al.: Synchronising EDML and NorthGRIP ice cores using δ 18 O of atmospheric oxygen (δ 18 O atm) and CH 4 measurements over MIS5 (80–123 kyr), Quaternary Science Reviews, 29, 222–234, 2010.

Chaovalitwongse, W. and Pardalos, P.: On the time series support vector machine using dynamic time warping kernel for brain activity classification, Cybernetics and Systems Analysis, 44, 125–138, 2008.

Cleveland, W. S. and Grosse, E.: Computational methods for local regression, Statistics and Computing, 1, 47–62, 1991.

Criel, J. and Tsiporkova, E.: Gene Time Eχpression Warper: a tool for alignment, template matching and visualization of gene expression time series, Bioinformatics, 22, 251–252, 2005.

Cuffey, K. and Paterson, W.: Physics of Glaciers, 4th Edn, 2010.

Dansgaard, W. and Johnsen, S.: A flow model and a time scale for the ice core from Camp Century, Greenland, Journal of Glaciology, 8, 215–223, 1969.

Frey, M. M., Bales, R. C., and McConnell, J. R.: Climate sensitivity of the century-scale hydrogen peroxide (H2O2) record preserved in 23 ice cores from West Antarctica, Journal of Geophysical Research: Atmospheres, 111, 2006.

Gilbert, J. M., Rybchenko, S. I., Hofe, R., Ell, S. R., Fagan, M. J., Moore, R. K., and Green, P.: Isolated word recognition of silent speech using magnetic implants and sensors, Medical engineering & physics, 32, 1189–1197, 2010.

Gillet-Chaulet, F., Gagliardini, O., Seddik, H., Nodet, M., Durand, G., Ritz, C., Zwinger, T., Greve, R., and Vaughan, D. G.: Greenland ice sheet contribution to sea-level rise from a new-generation ice-sheet model, The Cryosphere, 6, 1561–1576, 2012.

Herron, M. M. and Langway Jr, C. C.: Firn densification: an empirical model, Journal of Glaciology, 25, 373–385, 1980.

Hutterli, M. A., McConnell, J. R., Bales, R. C., and Stewart, R. W.: Sensitivity of hydrogen peroxide (H2O2) and formaldehyde (HCHO) preservation in snow to changing environmental conditions: Implications for ice core records, Journal of Geophysical Research: Atmospheres, 108, 2003.

Kolhe, S. R., Patil, P. M., et al.: Dynamic time warping based static hand printed signature verification, Journal of Pattern Recognition Research, 1, 52–65, 2009.

Latecki, L. J., Megalooikonomou, V., Wang, Q., and Yu, D.: An elastic partial shape matching technique, Pattern Recognition, 40, 3069–3080, 2007.

Legrand, B., Chang, C., Ong, S., Neo, S.-Y., and Palanisamy, N.: Chromosome classification using dynamic time warping, Pattern Recognition Letters, 29, 215–222, 2008.

Ligtenberg, S., Heilsen, M., and van de Broeke, M.: An improved semi-empirical model for the densification of Antarctic firn, The Cryosphere, 5, 809–819, 2011.

Masson-Delmotte, V., Dreyfus, G., Braconnot, P., Johnsen, S., Jouzel, J., Kageyama, M., Landais, A., Loutre, M.-F., Nouet, J., Parrenin, F., et al.: Past temperature reconstructions from deep ice cores: relevance for future climate change, 2006.

Nielsen, N.-P. V., Carstensen, J. M., and Smedsgaard, J.: Aligning of single and multiple wavelength chromatographic profiles for chemometric data analysis using correlation optimised warping, Journal of Chromatography A, 805, 17–35, 1998.

Nye, J.: The mechanics of glacier flow, Journal of Glaciology, 2, 82–93, 1952.

Nye, J.: Correction factor for accumulation measured by the thickness of the annual layers in an ice sheet, Journal of Glaciology, 4, 785–788, 1963.

https://doi.org/10.5194/tc-2020-342
Preprint. Discussion started: 5 January 2021

Passalacqua, O., Gagliardini, O., Parrenin, F., Todd, J., Gillet-Chaulet, F., and Ritz, C.: Performance and applicability of a 2.5-D ice-flow model in the vicinity of a dome, 2016.

Potocki, M., Mayewski, P. A., Kurbatov, A. V., Simoes, J. C., Dixon, D. A., Goodwin, I., Carleton, A. M., Handley, M. J., Jaña, R., and Korotkikh, E. V.: Recent increase in Antarctic Peninsula ice core uranium concentrations, Atmospheric Environment, 2016.

Pravdova, V., Walczak, B., and Massart, D.: A comparison of two algorithms for warping of analytical signals, Analytica Chimica Acta, 456, 77–92, 2002.

Rabiner, L., Rosenberg, A., and Levinson, S.: Considerations in dynamic time warping algorithms for discrete word recognition, IEEE Transactions on Acoustics, Speech, and Signal Processing, 26, 575–582, 1978.

Rolland, C.: Spatial and seasonal variations of air temperature lapse rates in Alpine regions, Journal of Climate, 16, 1032–1046, 2003.

Sakoe, H. and Chiba, S.: Dynamic programming algorithm optimization for spoken word recognition, IEEE transactions on acoustics, speech, and signal processing, 26, 43–49, 1978.

Sigg, A. and Neftel, A.: Seasonal variations in hydrogen peroxide in polar ice cores, Ann. Glaciol, 10, 157–162, 1988.

Steig, E. J., Mayewski, P. A., Dixon, D. A., Kaspari, S. D., Frey, M. M., Schneider, D. P., Arcone, S. A., Hamilton, G. S., Spikes, V., Albert, M., et al.: High-resolution ice cores from US ITASE (West Antarctica): Development and validation of chronologies and determination of precision and accuracy, Annals of Glaciology, 41, 77–84, 2005.

Thomas, E. R., Marshall, G. J., and McConnell, J. R.: A doubling in snow accumulation in the western Antarctic Peninsula since 1850, Geophysical research letters, 35, 2008.

Tomasi, G., Van Den Berg, F., and Andersson, C.: Correlation optimized warping and dynamic time warping as preprocessing methods for chromatographic data, Journal of Chemometrics, 18, 231–241, 2004.

Travassos, J. M., Martins, S. S., Simões, J. C., and Mansur, W. J.: Radar diffraction horizons in snow and firn due to a surficial vertical transfer of mass, Brazilian Journal of Geophysics, 36, 507–518, 2018.

Verbesselt, J., Hyndman, R., Newnham, G., and Culvenor, D.: Detecting trend and seasonal changes in satellite image time series, Remote sensing of Environment, 114, 106–115, 2010.

Vinther, B. M., Clausen, H. B., Johnsen, S. J., Rasmussen, S. O., Andersen, K. K., Buchardt, S. L., Dahl-Jensen, D., Seierstad, I. K., Siggaard-Andersen, M.-L., Steffensen, J. P., et al.: A synchronized dating of three Greenland ice cores throughout the Holocene, Journal of Geophysical Research: Atmospheres, 111, 2006.

Wang, K., Gasser, T., et al.: Alignment of curves by dynamic time warping, The annals of Statistics, 25, 1251–1276, 1997.

Xue, Z., Du, P., and Feng, L.: Phenology-driven land cover classification and trend analysis based on long-term remote sensing image series, IEEE Journal of Selected Topics in Applied Earth Observations and Remote Sensing, 7, 1142–1156, 2014.